


In the format provided by the authors and unedited.

Origin of strong-field-induced low-order harmonic generation in amorphous quartz

P. Jürgens ^{1,3}, B. Liewehr ^{2,3}, B. Kruse^{2,3}, C. Peltz ², D. Engel¹, A. Husakou¹, T. Witting¹, M. Ivanov ¹,
M. J. J. Vrakking ¹, T. Fennel ^{1,2}  and A. Mermillod-Blondin ¹ 

¹Max-Born-Institute for Nonlinear Optics and Short Pulse Spectroscopy, Berlin, Germany. ²Institute for Physics, University of Rostock, Rostock, Germany.

³These authors contributed equally: P. Jürgens, B. Liewehr, B. Kruse. e-mail: thomas.fennel@uni-rostock.de; mermillod@mbi-berlin.de

Origin of strong-field induced low-order harmonic generation in amorphous quartz - Supplementary Information

P. Jürgens^{1,*}, B. Liewehr^{2,*}, B. Kruse^{2,*}, C. Peltz², D. Engel¹, A. Husakou¹, T. Witting¹, M. Ivanov¹, M. J. J. Vrakking¹, T. Fennel^{1,2} & A. Mermillod-Blondin¹

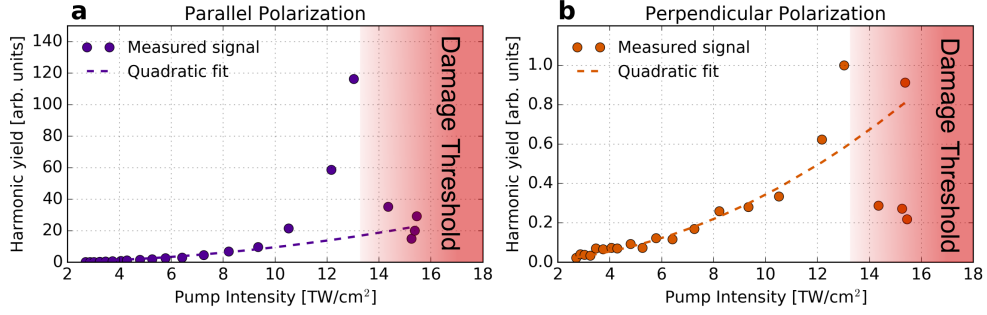
¹*Max-Born-Institute for Nonlinear Optics and Short Pulse Spectroscopy, Max-Born-Str. 2A, D-12489, Berlin, Germany*

²*Institute for Physics, University of Rostock, Albert-Einstein-Str. 23, D-18059, Rostock, Germany*

1 Pump intensity scans

For the experimental determination of the effective order of nonlinearity [see Fig. 4 in the main text] we performed measurements of the pump intensity dependence of the $n = 1$ harmonic yield for both parallel as well as in perpendicular pump probe polarizations. In both cases the detected harmonic yield is compared to the quadratic relationship expected from a third-order Kerr-type response. At small pump intensities the harmonic yield shows a perturbative character with a quadratic increase of the harmonic signal with pump intensity. In contrast, a strong deviation from the quadratic fit is observed for both parallel and perpendicular pump and probe polarizations above a certain threshold intensity. The threshold intensity where such a deviation from the perturbative scaling of the $n = 1$ harmonic yield occurs strongly depends on the relative pump probe polarization. In the case of parallel pump probe polarizations (see Fig. S1a), a clear departure from

*P.J., B.L. & B.K. contributed equally to this work



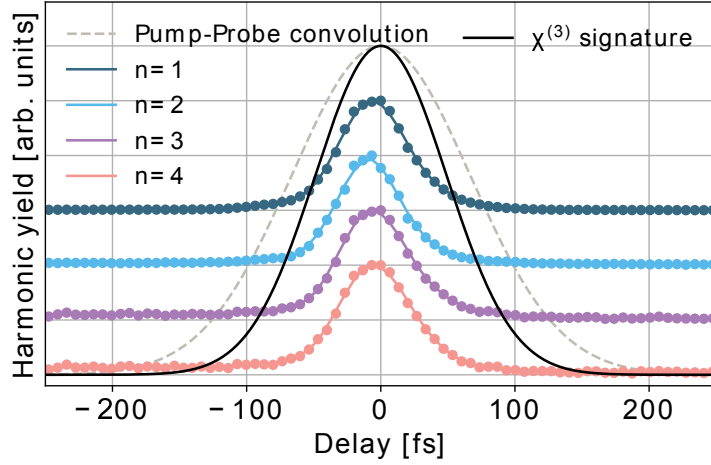
Supplementary Figure | S1: Pump intensity scans. **a**, Measured harmonic yield of the $n = 1$ harmonic depending on the peak intensity of the mid-IR pump laser pulse in a parallel polarization configuration compared to a quadratic increase of the harmonic signal. **b**, same as in **a** for pump and probe beams orthogonally polarized.

the perturbative scaling appears at $\approx 10 \text{ TW/cm}^2$ whereas orthogonally polarized pump and probe beams result in a departure from a quadratic harmonic yield at intensities $\approx 12 \text{ TW/cm}^2$ (as shown in Fig. S1b).

2 Temporal signature of the harmonic signal

As an alternative approach for the characterization of the frequency mixing process, the delay dependence of the detected harmonic emission is analyzed. Considering a pump-probe scenario with a strong pump and a weak probe laser pulse, the order of nonlinearity m of a perturbative process [see Eq. (2) in the main text] is reflected in the temporal signature of its response through the convolution

$$I_{\text{exp}}(\tau) \propto \int_{-\infty}^{\infty} I_{\text{pump}}(t)^{m-1} I_{\text{probe}}(t - \tau) dt, \quad (1)$$



Supplementary Figure | S2: Temporal signature of the harmonics. Projection of the first four harmonic orders on the delay axis compared to the linear pump-probe convolution and the expected temporal signature of a $\chi^{(3)}$ response according to Eq. 1. Experimental data for different harmonic orders are offset vertically for clarity. The pump intensity was $\approx 12 \text{ TW/cm}^2$.

where τ is the pump-probe delay and $I_{\text{pump}}(t)$ and $I_{\text{probe}}(t)$ are the intensity envelopes of the pump and probe fields, respectively. For smooth envelopes with only a single maximum, the term I_{pump}^{m-1} forms an increasingly narrow gate with increasing order that ultimately evolves into a delta function in the limit of infinitely high order m . This limiting case resembles the minimal width of the delay dependent signal that is given by the duration of the probe field. Generally, the effective temporal width τ_{eff} of a nonlinear signal on the delay axis reflects the order of the underlying nonlinear process and, when assuming gaussian envelopes, follows as

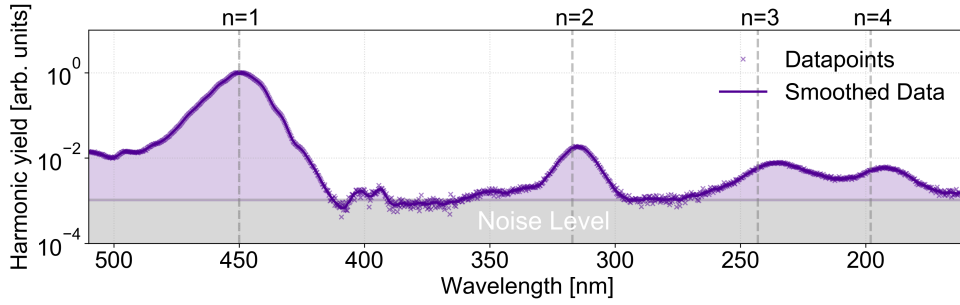
$$\tau_{\text{eff}} = \sqrt{\frac{\tau_{\text{pump}}^2}{m-1} + \tau_{\text{probe}}^2}, \quad (2)$$

where τ_{pump} and τ_{probe} are the durations of the pump and probe laser pulses, respectively.

For the simplest form of a Kerr-type four-wave mixing signal with $m = 3$, the pump intensity enters quadratically, in accordance to the scaling behavior found at low intensity in Fig. S1. The analysis of the temporal signature of the four harmonic orders shown in Fig. 2(b) of the main text is presented in Fig. S2. We emphasize that all four harmonic orders exhibit nearly the same temporal width, suggesting an origin with a similar order of nonlinearity. This order must be significantly higher than $m = 3$, as the signal transient is substantially narrower than the signature expected from a Kerr-type four-wave mixing signal (solid curve). The width of the measured signals for harmonics $n = 1..4$ in Fig. S2 is consistent with orders of nonlinearity in the range $m \gtrsim 10$. This conclusion is in good agreement with the experimental determination of the effective nonlinearity from the comparison of the two polarization configurations (see Fig. 4 in the main text).

3 Role of impact ionization

In order to determine whether impact ionization contributes to the harmonic emission, we examine the emission time as well as the temporal symmetry of the harmonic wave-mixing signals with respect to the field maximum. If present, the signature of the self-accelerating nature of an impact-avalanche would translate into a different signal yield on the rising and trailing edges of the pump laser pulse, i.e. in asymmetric features in Fig. S2. As our experimental data shows a symmetric structure of the harmonics $n = 1..4$, peaked at the pump-probe overlap (see also Fig. 2b of the main text) that is not shifted over the examined intensity range, we rule out wave-mixing through impact ionization as an important contribution to the observed harmonics and thus attribute the

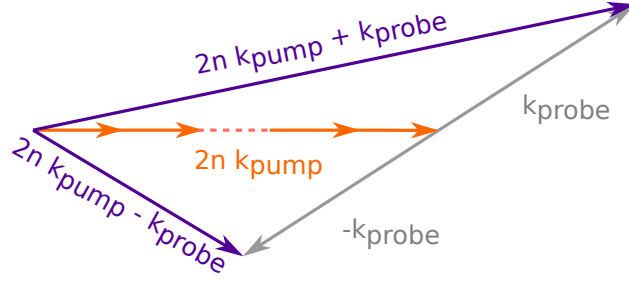


Supplementary Figure | S3: Spectral decay of injection harmonics. Projection of the time-resolved harmonic spectrum on the wavelength axis at the pump-probe overlap. The pump intensity was $\approx 12 \text{ TW/cm}^2$.

ionization-related signal to strong-field ionization.

4 Spectral decay of injection harmonics

In contrast to field-induced intraband harmonics and interband recombination harmonics, injection harmonics do not exhibit a plateau-like behavior. Analogous to conventional Brunel harmonics (which are also linked to the nonlinearity of the ionization rate), the harmonic yield of injection harmonics rapidly decays with their order ¹. Such a rapid decay clearly appears in the experimental results (see Fig. S3). Therefore, injection harmonics are not expected to strongly affect the high energy part of the harmonic spectrum that is dominated by interband recombination and/or intraband anharmonicity effects.



Supplementary Figure | S4: Propagation direction of sum- (top) and difference- (bottom) frequency generation components. The harmonics of the pump and probe beams (not represented) are collinear with respect to the pump and the probe, respectively.

5 Angular selection of the harmonics

Satisfying the phase-matching condition implies different emission directions for the sum- and the difference-frequency generation components, as illustrated in Fig. S4. By placing the spectrometer in the direction of emission of the sum-frequency components, difference-frequency signals (at the frequencies $2n \times \omega_{\text{pump}} - \omega_{\text{probe}}$) as well as the third harmonic from the pump laser pulse are not recorded, since these signals are emitted at angles outside the acceptance cone of the experimental apparatus employed for the spectroscopic analysis (see Extended Data Fig. 1).

We emphasize that the isolated features around 410 nm visible in Fig. 2b (see main manuscript) are emitted from the optical parametric amplifier (at a wavelength corresponding to the 2nd harmonic of the pump laser).

6 Polarization measurement

As detailed below, our numerical model predicts that in a cross-polarized geometry the polarization of the harmonic radiation corresponds to the polarization of the NIR probe laser pulse. In order to verify this prediction we measured the relative polarization of the pump and probe laser pulses and the harmonic radiation, respectively. The measurement was carried out in amorphous quartz (a-SiO₂). The transmission of the respective radiation through a broadband polarization filter (placed between L1 and BS, see Extended Data Fig. 1) as a function of the polarizer angle (see Fig. S5) confirms that the $n = 1$ harmonic has the same polarization as the probe laser pulse, while the pump laser pulse is orthogonally polarized.

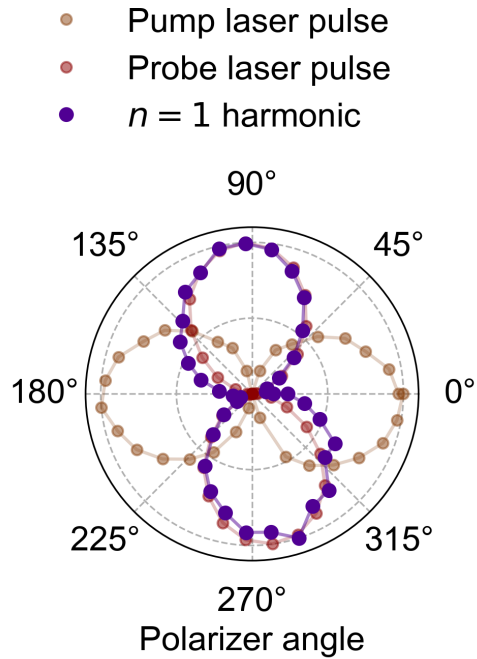
Furthermore, the anisotropic character of the wave mixing signal at low intensity shows that propagation effects do not remove the possibility to observe orientation dependent signal.

7 Polarization dependence and effective order of nonlinearity

When considering an instantaneous m^{th} order nonlinear process in an isotropic medium, the associated polarization can be expressed in the general form

$$\mathbf{P} = \varepsilon_0 \chi^{(m)} (\mathbf{E} \cdot \mathbf{E})^\mu \mathbf{E} , \quad (3)$$

as discussed in the main text. In what follows, we explain how the order of nonlinearity $m = 2\mu + 1$ can be directly extracted from the nonlinear signal obtained for the two polarization configurations



Supplementary Figure | S5: Intensity of the harmonic $n = 1$ in a-SiO₂ as a function of the polarizer angle. The polarization of the harmonic radiation clearly follows the polarization of the probe laser pulse in a cross-polarized pump-probe scenario for $I_{\text{pump}} = 12 \text{ TW/cm}^2$ and $I_{\text{probe}} = 0.015 \text{ TW/cm}^2$.

in the pump-probe experiment. We consider a strong pump pulse \mathbf{E}_{pump} and a weaker probe field $\mathbf{E}_{\text{probe}}$, forming together the total input field

$$\mathbf{E} = \mathbf{E}_{\text{pump}} + \mathbf{E}_{\text{probe}} = \frac{\hat{\mathbf{E}}_{\text{pump}}}{2} e^{i\omega_{\text{pump}}t} + \frac{\hat{\mathbf{E}}_{\text{probe}}}{2} e^{i\omega_{\text{probe}}t} + c.c. \quad (4)$$

with the carrier waves being described by the exponentials and assuming that the amplitudes $\hat{\mathbf{E}}_{\text{pump,probe}}$ contain the polarization direction of the two fields. Inserting the total field into Eq. (3) and inspecting only terms in the nonlinear polarization that are linear in the probe field one finds that the amplitude $\hat{\mathbf{E}}_{\text{probe}}$ can in principle appear in any of the m occurrences of the total field, leading to m equivalent contributions. In the perpendicular case, however, the probe field can contribute only, if it appears in the last factor on the right hand side. When appearing in the other factor $(\mathbf{E} \cdot \mathbf{E})^\mu$, the contribution will vanish because of the vanishing projection of the perpendicularly polarized fields. As a result, only one realization is active in the perpendicular case.

Combining the above considerations, the polarization is m -fold enhanced in the parallel configuration. Expressed in terms of the intensities I_{\parallel} and I_{\perp} of the polarization (or of the corresponding emission), the yield ratio is thus connected to the order of nonlinearity via

$$I_{\parallel} = m^2 I_{\perp}, \quad (5)$$

which is the relation used for the analysis discussed in the main text.

8 Simulation of the harmonic signals

The numerical modelling of the wave mixing departs from the time derivative of the current density (dipole acceleration density) associated with the injection-induced response

$$\dot{\mathbf{J}} = q_e n_0 \left[\frac{q_e}{m_e} \mathbf{E} \rho + \mathbf{v}_0 \dot{\rho} + \frac{\partial}{\partial t} (\mathbf{x}_0 \dot{\rho}) \right], \quad (6)$$

as introduced in the main text. Here $q_e = -e$ is the electron charge, m_e the mass, \mathbf{E} the laser field, ρ the electron density in the conduction band normalized to the molecular density n_0 , \mathbf{v}_0 the injection velocity, $\mathbf{x}_0 = \frac{E_g}{q_e} \frac{\mathbf{E}}{E^2}$ the injection displacement, and E_g the bandgap energy. For our SiO_2 sample we used $n_0 = 2.2 \times 10^{22} \text{ cm}^{-3}$. The conduction band electron density is modified by electron transfer from the valence band. This transfer is described by

$$\dot{\rho} = \Gamma(|\mathbf{E}|) = (1 - \rho) \Gamma_{\text{ADK}}(|\mathbf{E}|), \quad (7)$$

where the transfer rate Γ is modelled with a saturation term multiplied with a Ammosov-Delone-Krainov tunneling rate ² evaluated for actual laser field and using the bandgap energy. Note that the injection velocity is set to $\mathbf{v}_0 = 0$. Finally, the total acceleration is calculated by adding the respective term from the Kerr response

$$\dot{\mathbf{J}}_{\text{Kerr}} = \chi^{(3)} \frac{\partial^2}{\partial t^2} |\mathbf{E}|^2 \mathbf{E}, \quad (8)$$

where we use $\chi^{(3)} = 1.9 \times 10^{-22} \text{ m}^2\text{V}^{-2}$, as determined from the nonlinear refractive index given in Ref. 3. The time-evolution of the conduction band population and the total acceleration density is calculated on a temporal grid with time step of $\Delta t = 5 \text{ as}$. The harmonic signals are extracted from the corresponding spectral intensity after Fourier transformation and spectral integration over the peaks of the individual harmonic orders. For the selective analysis shown in Fig. 4 in the main text, the spectral intensities of the individual contributions are analyzed.

1. Brunel, F. Harmonic generation due to plasma effects in a gas undergoing multiphoton ionization in the high-intensity limit. *J. Opt. Soc. Am. B* **7**, 521–526 (1990).
2. Ammosov, M. V., Delone, N. B. & Krainov, V. P. Tunnel ionization of complex atoms and of atomic ions in an alternating electromagnetic field. *Sov. Phys. JETP* **64**, 1191–1194 (1986).
3. Agrawal, G. (ed.) *Nonlinear Fiber Optics*. Optics and Photonics (Academic Press, Boston, 2013).